

High-Resolution Electronic Spectroscopy of the Doorway States to Intramolecular Charge Transfer

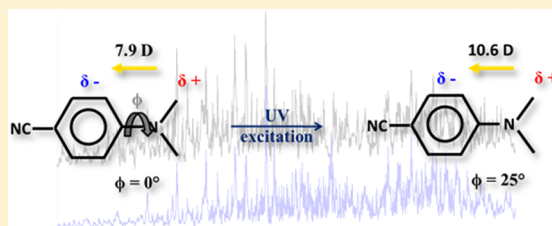
Adam J. Fleisher,^{†,‡} Ryan G. Bird,[†] Daniel P. Zaleski,[§] Brooks H. Pate,[§] and David W. Pratt^{*,†,‡,§}

[†]Department of Chemistry, University of Pittsburgh, Pittsburgh, Pennsylvania 15260, United States

[§]Department of Chemistry, University of Virginia, Charlottesville, Virginia 22904, United States

S Supporting Information

ABSTRACT: Reported here are several of the ground, first, and second excited state structures and dipole moments of three benchmark intramolecular charge transfer (ICT) systems; 4-(1H-pyrrol-1-yl)benzonitrile (PBN), 4,4'-dimethylaminobenzonitrile (DMABN), and 4-(1-pyrrolidinyl)benzonitrile (PYRBN), isolated in the gas phase and probed by rotationally resolved spectroscopy in a molecular beam. The related molecules 1-phenylpyrrole (PP) and 4-aminobenzonitrile (ABN) also are discussed. We find that the S_1 electronic state is of B symmetry in all five molecules. In PBN, a second excited state (S_2) of A symmetry is found only $\sim 400\text{ cm}^{-1}$ above the presumed origin of the S_1 state. The change in dipole moment upon excitation to the A state is measured to be $\Delta\mu \approx 3.0\text{ D}$, significantly smaller than the value predicted by theory and also smaller than that observed for the “anomalous” ICT band of PBN in solution. The B state dipole moments of DMABN and PYRBN are large, $\sim 10.6\text{ D}$, slightly larger than those attributed to “normal” LE fluorescence in solution. In addition, we find the unsaturated donor molecules (PP, PBN) to be twisted in their ground states and to become more planar upon excitation, even in the A state, whereas the saturated donor molecules (ABN, DMABN, PYRBN), initially planar, either remain planar or become more twisted in their excited states. It thus appears that the model that is appropriate for describing ICT in these systems depends on the geometry of the ground state.



INTRODUCTION

From simple redox reactions such as $2\text{Na} + \text{Cl}_2 \rightarrow 2\text{NaCl}$ to more complex ones that play significant roles in processes as diverse as natural photosynthesis and commercial photovoltaic cells, charge transfer (CT) lies at the very heart of chemistry. We consider here a particular class of CT reactions, excited state intramolecular charge transfer (ICT) reactions, in which a fraction of the electronic charge is transferred from one part of a large molecule to another part of the same molecule by irradiation with UV light (for a review, see ref 1). ICT reactions were initially observed in the condensed phase, where excitation of certain molecules with a single wavelength of light yielded emission at two wavelengths, a shorter wavelength (often unshifted) emission that was attributed to a locally excited (LE) state, and a longer wavelength (Stokes-shifted) emission that was attributed to an ICT state. The relative intensity of the two emissions was found to depend on the conformational degrees of freedom of the excited species, leading to the concepts of twisted ICT (TICT) and planarized ICT (PICT) states. Polar solvents were found to enhance the ICT emissions of both types of states and to shift them to longer wavelengths.

One common use of solvent effects is to determine the permanent electric dipole moments (EDMs) of the electronically excited states of many ICT molecules, employing the Lippert equation.² Another common use of solvent effects has been to determine the polarity of a probe binding site when an

ICT molecule is attached to a protein, membrane, or other macromolecule. But all such determinations rely on three key assumptions: that the excited state of the fluorophore is fully relaxed before it emits light, that CT from the donor to the acceptor (where it occurs) is complete, and that there are no specific interactions between the fluorophore and its environment that might affect the wavelength or the intensity of the emission. Additionally, other “higher-order” effects, such as differently oriented ground and excited state EDMs and the induced dipoles produced by interactions between the solute and the solvent, also are ignored.

Recent theoretical work has shown that TICT and PICT “states” are, in fact, only stationary points on the potential energy surface (PES) of a single ICT state and may be either minima or maxima (transition states).^{3–5} The barriers separating them are very small, so at room temperature, they both may be populated. But the electronic structure of the single ICT state is different from that of the LE state, so an adiabatic reaction pathway (ARP) connects them. Further complicating matters is the existence of other PESs (and ARPs) at higher energies, necessitating the use of state labels to

Special Issue: Paul F. Barbara Memorial Issue

Received: April 29, 2012

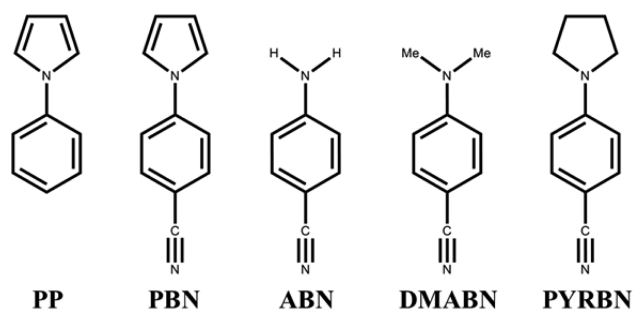
Revised: August 7, 2012

Published: August 22, 2012

describe the different geometries. Nonadiabatic transitions from the ARP on one state to that on another occur at conical intersections. The geometries associated with such crossings also are a subject of much debate.

Reported here are high-resolution electronic spectroscopy experiments on isolated donor–acceptor molecules in a collision-free molecular beam in the absence of a perturbing solvent environment. We aim to test whether the intrinsic properties of ICT molecules in their electronically excited states can be reliably extracted from condensed phase experiments or whether the properties of such species in the gas phase are different. A central question is the extent to which the Franck–Condon (FC) accessible, lowest-energy excited state has progressed along the ARP connecting the S_1 LE and ICT states. Our test molecules include both TICT and PICT “species” (see Chart 1). The determined properties of these

Chart 1. Structures of Benchmark 4-Aminobenzonitriles



species include the energies of their lowest excited states, their electronic character, their geometries, and their permanent EDMs, measured by performing Stark-effect studies of their rotationally resolved spectra. These measurements also provide intricate molecular detail that may be directly compared with high-level theoretical calculations of the PESs of ground and electronically excited states.

METHODS

High-resolution fluorescence excitation spectra (FES) of 4-(1H-pyrrol-1-yl)benzonitrile (PBN), 4,4'-dimethylaminobenzonitrile (DMABN), and 4-(1-pyrrolidinyl)benzonitrile (PYRBN) were independently recorded in a cold molecular beam environment using an ultraviolet laser. The laser system, consisting of an Ar⁺-pumped ring dye laser and external frequency doubling cavity, has been described elsewhere.^{6–9} For PBN, rhodamine 590 (R6G) laser dye was used to create fundamental visible laser radiation, which was frequency-doubled into the UV with a BBO crystal housed in a delta-type cavity. The PBN spectra were recorded using an average laser power of 300 μ W. For DMABN and PYRBN, mixtures of DCM and Kiton Red laser dyes were used to create the fundamental radiation. Again, a BBO crystal and delta cavity were used for frequency-doubling, creating average output powers of 250 and 60 μ W in the UV for DMABN and PYRBN, respectively. All experiments required a laser scan speed of 15 MHz/s over a range of 120 GHz (4 cm^{-1}) to obtain an acceptable signal-to-noise ratio. For DMABN, it also was necessary to record an additional 15 GHz (0.5 cm^{-1}) section of several Stark spectra at the slower scan speed of 3.75 MHz/s. Along with the FES, the absorption spectrum of I_2 and frequency markers from a temperature-stabilized Fabry–Pérot interferometer were recorded for absolute and relative

frequency calibration using jba95 acquisition software and a small amount of fundamental visible laser light.¹⁰ Both field free and Stark spectra were analyzed manually using jb95 simulation software.¹¹

Each sample required different source conditions to successfully seed a stream of Ar backing gas. PBN was heated to 145 $^{\circ}\text{C}$ in a quartz source and then expanded at a total backing pressure of 320 Torr through a 200 μm pinhole into a vacuum chamber (10^{-5} Torr). This supersonic expansion was skimmed while entering a second vacuum chamber (10^{-7} Torr), creating the molecular beam. The collisionless molecular beam was crossed at a right angle by the UV laser, and total fluorescence following excitation was recorded by a PMT and photon counting system mounted perpendicular to both the laser and molecular beam. Spherical mirrors and wire mesh Stark plates mounted above and below the intersecting beams were used to collect fluorescence and, when desired, create a homogeneous electric field. In the PYRBN experiments, the sample was heated to 175 $^{\circ}\text{C}$ and expanded in Ar at a total backing pressure of 455 Torr. Both PBN and PYRBN were purchased from Maybridge (Thermo Fisher Scientific) and used without further purification. DMABN, purchased from Aldrich, was heated to 200 $^{\circ}\text{C}$ and expanded in Ar at a total backing pressure of 380 Torr.

Microwave spectra of PBN were collected using the chirped-pulse Fourier transform microwave (CP-FTMW) spectrometer described previously.¹² PBN was heated to 120 $^{\circ}\text{C}$ and expanded through a pulsed nozzle at 10 Hz along with 1 kTorr of He backing gas. The entire spectrum was recorded from 6.5 to 17 GHz in 450 MHz segments, each of which was measured by collecting a 10 μs free induction decay (FID) and signal-averaging for up to 5000 shots. The segments were then patched together, and 120 μa -type transitions were assigned and analyzed using jb95 software.

The microwave Stark spectrum of DMABN was collected using a CP-FTMW spectrometer¹³ containing a Stark cage.¹⁴ DMABN was heated to 130 $^{\circ}\text{C}$ and expanded through a single nozzle at 7 Hz with 760 Torr Ne backing gas. The spectrum was recorded from 6.5 to 18.5 GHz at an applied electric field of 20 V/cm and signal-averaged over 3.5×10^5 nozzle pulses. Individual line assignments were made in the QSTARK program^{15,16} and then simulated for visual comparison with experiment using jb95 software. Field calibration procedures are described in the Supporting Information (SI) section.

Theoretical work in support of the experiments was performed using Gaussian 03 (revision E.01) software¹⁷ at the University of Pittsburgh Center for Simulation and Modeling (SAM). Ground state geometries were optimized using the M05-2X hybrid density functional with the 6-31+G* basis set. Dipole moments were then calculated using MP2/ aug-cc-pVTZ on the previously optimized geometries. For comparison with calculations available in the literature, complete active space self-consistent field (CASSCF) point calculations of PYRBN were performed with an active space of 12 electrons and 10 orbitals (all π and π^*) using the D95 V basis set.¹⁸ Only the relevant results of the CASSCF calculations are presented here; further details are available in the SI.

RESULTS AND INTERPRETATION

4-(1H-Pyrrol-1-yl)benzonitrile. Figure 1 shows the low-resolution FES of PBN entrained in a supersonic jet previously observed by Belau et al.¹⁹ It exhibits weakly fluorescent S_1 – S_0

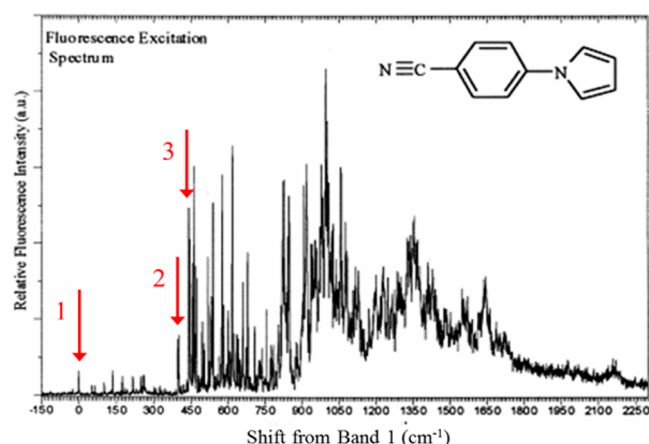


Figure 1. Vibrationally resolved fluorescence excitation spectrum (FES) of PBN (ref 19.). The red arrows labeled 1, 2, and 3 indicate the bands studied at high resolution.

transitions, similar to the jet-cooled spectrum of PP;^{19,20} however, at energies only 400 cm⁻¹ above the lowest frequency PBN band, a substantial increase in fluorescence intensity is observed. This has been attributed to the influence of a second excited state (*S*₂) with a greater fluorescence quantum yield than *S*₁.¹⁹ To determine whether this explanation is correct, high-resolution spectra were recorded of bands marked 1, 2, and 3 in Figure 1. These are shown in Figures 2–4.

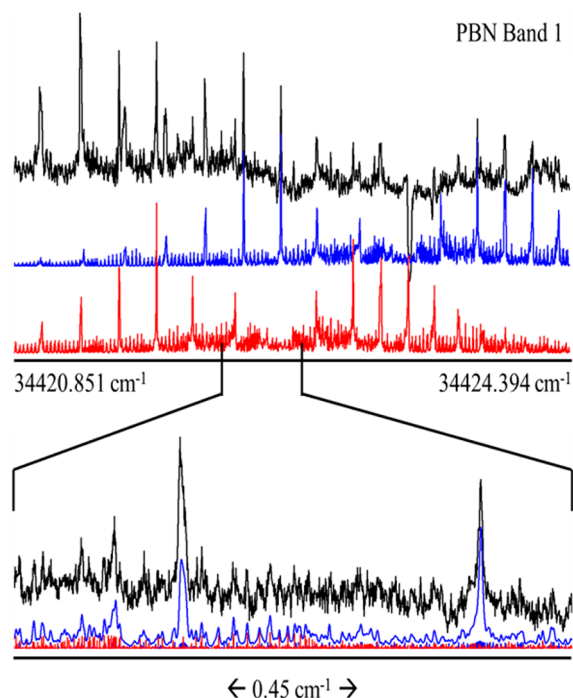


Figure 2. Rotationally resolved FES of PBN band 1. The experimental trace shown in black was fit to two simulations, shown below in blue and red.

Band 1 is the lowest energy electronic transition observed in the low resolution spectrum. Its relatively low fluorescence intensity was confirmed in our experiments. At high resolution, band 1 actually consists of two weak subbands of similar intensity, as seen in Figure 2, labeled band 1 red (lower energy) and band 1 blue (higher energy) from this point forward. (As

will be discussed later, the existence of two subbands in this spectrum provides evidence for a tunneling motion between two equivalent minima along the twisting coordinate of PBN.) In contrast, the rotationally resolved FES of PBN at +400 (band 2) and +422 cm⁻¹ (band 3) consist of only single strong bands, as shown in Figures 3 and 4.

These data were analyzed using the following procedure: First, anticipating that the near-prolate symmetric top nature of PBN would limit the accuracy of the *a*-type electronic spectral analysis, ground state rotational constants of PBN were determined from a fit to Watson's A-reduced Hamiltonian²¹ of an independently measured microwave spectrum (see SI).

PBN Band 2

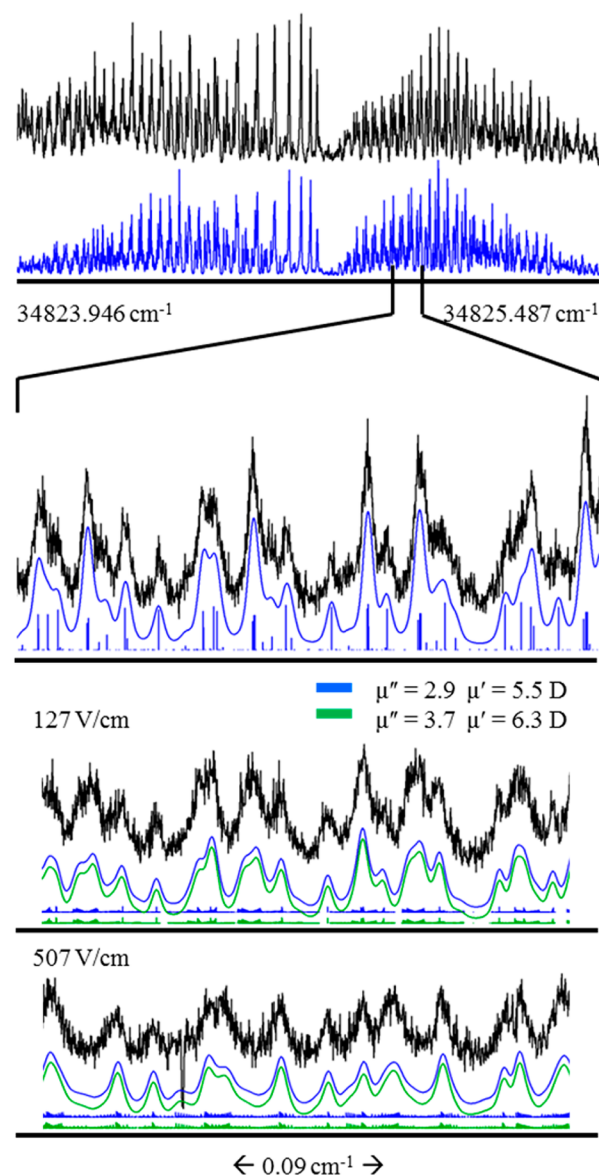


Figure 3. Rotationally resolved FES of PBN band 2. The experimental trace shown in black was fit to a single simulation, shown in blue. The bottom two panels show the effects of an applied electric field on the high resolution spectrum. The blue and green simulations of the Stark spectra appear identical, thereby illustrating the difficulty encountered when attempting to independently determine the permanent electric dipole moment (EDM) of each electronic state.

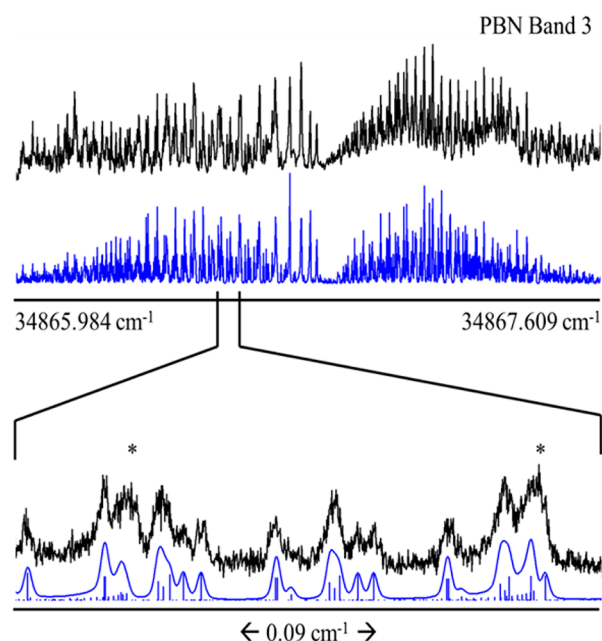


Figure 4. Rotationally resolved FES of PBN band 3. The two asterisks identify regions of unassigned intensity found in the experimental spectrum (black trace) that are not accounted for by the simulation (blue trace). The presence of a second weak electronic band is suspected, as more of these “extra peaks” appear throughout the spectrum of PBN band 3.

Next, excited state rotational constants of PBN were determined from fits to rigid-rotor Hamiltonians of the observed rotational structure in each of the spectra in Figures 2–4 using the program *jb95*. In these fits, ground state constants were kept fixed to their microwave values, and excited state constants were varied in a least-squares fashion to minimize differences between observed and calculated frequencies. More than 60 resolved transitions were fit in the electronic spectrum of band 1, and more than 130 resolved transitions were fit in the electronic spectra of bands 2 and 3. The combined microwave and high-resolution FES data for all observed PBN bands are summarized in Table 1.

To aid in the determination of molecular structure from the measured inertial parameters, the S_0 geometry of PBN was optimized using M05-2X density functional theory and the 6-31+G* basis set. The rotational constants of the optimized structure ($A = 3508.2$, $B = 383.3$, and $C = 351.7$ MHz) are in good agreement with the microwave values listed in Table 1.

Notably, this structure has a large negative inertial defect, $\Delta I = -21.6 \mu\text{Å}^2$, which decreases substantially in magnitude when PBN is excited by light, to values of $\sim -7 \mu\text{Å}^2$ in bands 1 and 2 and $\sim -4 \mu\text{Å}^2$ in band 3. Figure 5 shows a plot of ΔI vs ϕ as

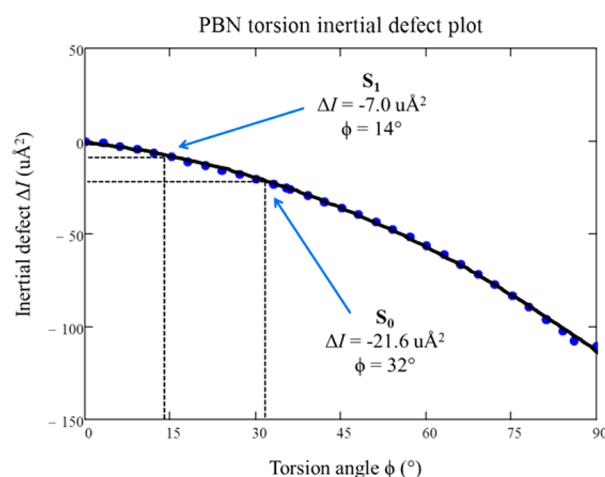


Figure 5. Plot of ΔI vs. ϕ as calculated from the ground state torsional PES shown in Figure S5 (blue data points, see SI). These data points were fit to a second-order polynomial (black curve) and used to determine ϕ for all PBN electronic states. The S_0 and S_1 interpolations are shown in the figure.

calculated by DFT (see SI for details). This plot reveals that ground state PBN is twisted about the bond connecting the two rings by an equilibrium angle of 32° and that the corresponding twist angles in the excited state(s) are 14° in band 1, 13° in band 2, and 9° in band 3. The theoretical barrier to ring planarity at $\phi = 0^\circ$ is $V''(0^\circ) = 469 \text{ cm}^{-1}$, whereas the barrier to ring perpendicularity at $\phi = 90^\circ$ is $V''(90^\circ) = 1003 \text{ cm}^{-1}$. We believe that the splitting found in band 1 is a consequence of hindered internal rotation about the bond connecting the two unsaturated rings in the excited S_1 state, resulting from a decrease in one or both of the barrier heights mentioned above. Importantly, the high resolution spectra of bands 2 and 3 show no such splittings, showing that the ground state is not involved.

The second significant result on PBN is the detection of the origin of the S_2 state. Recall that PBN exhibits increased fluorescence intensity at about 400 cm^{-1} above band 1, in the vicinity of bands 2 and 3. We find that the electronic transition moment (ETM) in (both subbands of) band 1 lies close to the b inertial axis, since this band is a hybrid band with 87% b

Table 1. Experimental Inertial Parameters Derived from the Microwave and UV Spectra of PBN^a

parameter	S_0	band 1 red	band 1 blue	band 2	band 3
A (MHz)	3492.2(2)	3376.2(1)	3376.0(1)	3388.1(1)	3387.7(1)
B (MHz)	382.6028(4)	384.4(1)	384.5(1)	384.5(1)	384.5(1)
C (MHz)	349.9721(4)	346.8(1)	346.8(1)	346.9(1)	346.3(1)
ΔI ($\mu\text{Å}^2$)	-21.559(8)	-7.0(5)	-7.0(5)	-6.7(5)	-4.5(5)
κ	-0.979	-0.975	-0.975	-0.975	-0.975
assigned lines	120	66	65	137	254
OMC (MHz)	0.032	6.5	6.6	3.8	6.3
origin (cm^{-1})		34422.599(1)	34423.352(1)	34824.753(1)	34866.829(1)
ETM ($a/b/c$; %)		0/87/13	0/87/13	100/0/0	100/0/0
fwhm (L/G; MHz)		30/35	30/35	30/35	30/30

^aColumns with the headings “band 1”, etc. contain the excited electronic state (S_1) parameters of each respective transition studied in Figure 1.

character and 13% c character; see Table 1. In contrast, bands 2 and 3 are 100% a -type; the ETMs of these bands are parallel to the a inertial axis, the long axis of PBN. 1L_b states of benzene derivatives exhibit b -type spectra, whereas 1L_a states exhibit a -type spectra.²² Thus, the observation of a change in the orientation of the ETM with increasing excitation energy in PBN shows that a second electronic state is responsible for the increased fluorescence intensity at $\sim 400\text{ cm}^{-1}$, confirming the proposal of Belau et al.¹⁹ We therefore assign band 1 as an excitation to the 1L_b state, and bands 2 and 3 as excitations to the 1L_a state. The 1L_a electronic state is often considered to be the state responsible for charge transfer in polar solvents. [The existence of c -type transitions in band 1 is a result of the benzene ring twisting out of the ab inertial plane by a vibrationally averaged angle τ of $\sim 21^\circ \pm 3^\circ$ (where $\tan \tau = (c/b)^{1/2}$), similar to that observed previously in the case of PP.²³]

Given the difference in the electronic nature of the 1L_a and 1L_b states, it was of interest to measure the difference in their permanent electric dipole moments (EDMs) using an external electric field. The experimental Stark spectra of both bands 2 and 3 were recorded over the range 42–507 V/cm and fit with several effectively identical simulations, as seen for the case of band 2 in Figure 3. A high linear correlation was observed between the ETMs of the two electronic states, owing to the fact that only a -type rovibronic transitions were observed. An analysis of this correlation (see SI) shows that by fixing the ground state value of the EDM to the theoretical value of 3.43 D, the best excited state values are $\mu'(^1L_a) = 6.0\text{ D}$ for band 2, and $\mu'(^1L_a) = 6.3\text{ D}$ for band 3. Unfortunately, owing to the low fluorescence intensity, the excited state value for band 1 could not be measured; the calculated value for the 1L_b state is 2.8 D.⁵

4,4'-Dimethylaminobenzonitrile. Similar experiments were performed on DMABN. In this case, a different strategy was used for their analysis because the rotationally resolved electronic spectra are extremely congested owing to multiple overlapping torsional subbands that result from methyl group torsional motions.²⁴ Thus, CP-FTMW experiments were first performed to study the microwave spectrum of DMABN in the gas phase; the results of these measurements, which include a substitution structure determined by detection of all ^{13}C and ^{15}N isotopologues in natural abundance, are reported elsewhere.²⁵ Next, the microwave spectrum of DMABN was recorded again in the presence of an electric field, generated using the parallel-plate configuration of a Stark cage; see the SI for a typical example and a listing of all line assignments. A fit of 30 rotational transitions by linear least-squares yields a value of $\mu_a = 7.9\text{ D}$ for the ground state EDM of DMABN in the gas phase. Then the rotationally resolved electronic spectrum of band 5 in the S_1 – S_0 transition of DMABN²¹ was examined at applied electric fields lying between 42 and 846 V/cm. Figure 6 shows a typical example, the entire spectrum recorded over $\sim 3.4\text{ cm}^{-1}$ at an applied electric field of 507 V/cm. As is apparent, the assignment of individual rotational transitions was nearly impossible in this spectrum, owing to the extreme congestion. However, a few moderately well resolved lines could be followed within the A subband of this spectrum (blue sticks in Figure 6), leading to the assignment of 20 transitions. While holding μ_a fixed to its ground state value (see SI for details), a least-squares fit of these transitions to experiment produced a value of $\mu_a = 10.6\text{ D}$ for the electronically excited state, with an OMC of 14.8 MHz (well below the experimental line width of about 55 MHz). The same EDMs were then used

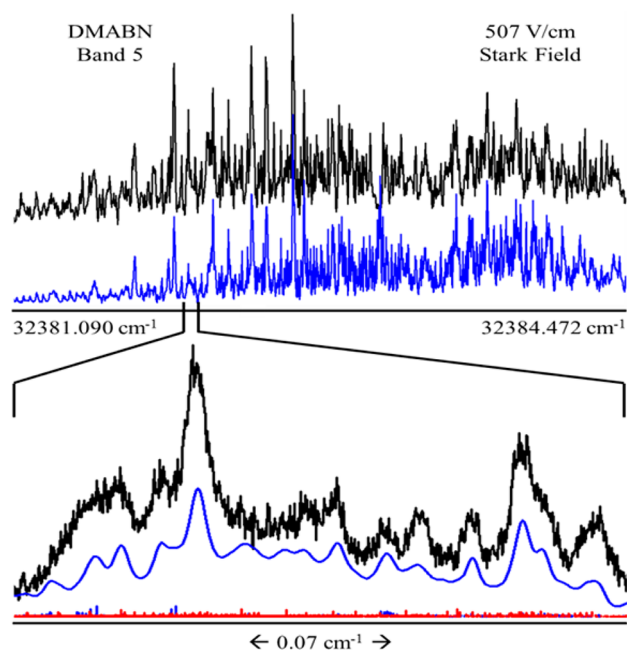


Figure 6. Rotationally resolved FES of band 5 of DMABN recorded at an applied electric field of 507 V/cm. The experimental trace is shown in black, and the combined simulation of both the A (blue sticks) and G (red sticks) subbands is shown in blue.

to simulate the G subband (red sticks), and a convolution of the A and G subbands that includes line width contributions from Gaussian (30 MHz) and Lorentzian (35 MHz) line shapes is shown for comparison with the experimental trace (black). As in the earlier experiments,²⁴ the E subband that must also be present in these spectra was not included in the simulations.

4-(1-Pyrrolidinyl)benzonitrile. The low-resolution FES of PYRBN is fundamentally different from those observed for the phenylpyrroles.^{26,27} The lowest frequency band in PYRBN (the S_1 – S_0 origin) is the most intense transition in the entire spectrum, and the strong low-frequency vibrational progressions that appear in the corresponding spectra of the phenylpyrroles are absent. Clearly, the energy separation of the S_1 and S_2 states—and perhaps their identities, as well—must be very different in PYRBN.

High resolution FES of PYRBN were recorded to explore this issue. Figure 7 shows the entire recorded spectrum of the origin band, which spans approximately 3 cm^{-1} . Exactly 200 rotational transitions in the resolved spectrum were assigned using pure b -type selection rules and fit in a linear least-squares fashion to the experiment. Table 2 reports the rotational constants and electronic origin frequency, among other parameters, determined from this fit. As clearly indicated by the observed b -type selection rules, the gas phase S_1 state of PYRBN is assigned as the 1L_b state.

The ground state inertial defect (ΔI) derived from the experimentally determined rotational constants of PYRBN is $-21.1\text{ }\mu\text{Å}^2$, qualitatively similar to the $\Delta I''$ values of PP²³ and PBN (-26.9 and $-21.6\text{ }\mu\text{Å}^2$, respectively). However, the reason for this similarity is not the same as that found for PP and PBN. In PYRBN, the saturated pyrrolidine ring is puckered, resulting in heavy atom displacements above and below the phenyl ring plane. This saturated ring nonplanarity results in a large negative $\Delta I''$. In contrast, the similar $\Delta I''$ values in PP and PBN

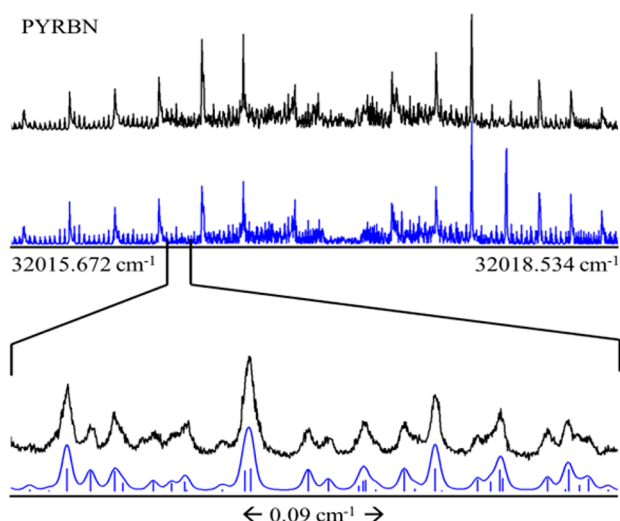


Figure 7. Rotationally resolved FES of the S_1 origin band in PYRBN. The experimental trace is shown in black, and the simulation is shown in blue.

Table 2. Experimental Inertial Parameters Derived from the UV Spectrum of PYRBN^a

parameter	theory	S_0	S_1
A (MHz)	3097.6	3083.0(1)	3005.7(1)
B (MHz)	366.7	366.1(1)	367.2(1)
C (MHz)	332.3	331.8(1)	331.7(1)
ΔI ($\mu\text{Å}^2$)	−20.5	−21.1(6)	−20.8(6)
κ	−0.975	−0.975	−0.973
assigned lines		200	
OMC (MHz)		2.9	
origin (cm^{-1})		32017.232(1)	
ETM (a/b/c; %)		0/100/0	
fwhm (L/G; MHz)		20/30	

^aThe theoretical ground state structure was optimized using M05-2X/6-31+G*.

are due to substantial twisting between the planar unsaturated rings in the phenylpyrroles. (Comparatively, the inertial defect of the puckered equatorial conformer of pyrrolidine was determined from its rotational spectrum in a supersonic jet to be $\Delta I'' = -18.5 \mu\text{Å}^2$.²⁸) In addition, no c -type transitions were found in the spectrum of PYRBN. Their presence in the S_1 – S_0 spectra of PP and PBN are a clear indication of significant ring torsion in the vibrationally averaged structures of those systems, something only minimally present in the structure of PYRBN. The calculated twist angle of PYRBN predicted by hybrid DFT (M05-2X/6-31+G*) is 6° in the ground state, small compared with the phenylpyrroles; the associated theoretical rotational constants are listed in Table 2.

Very little change in the B or C rotational constants is observed upon excitation of PYRBN, whereas a decrease in A (due to benzene ring expansion upon excitation) was measured. (This also accounts for the very symmetric nature of its high resolution spectrum, Figure 7.) More telling are the nearly identical ΔI values measured for each electronic state: $\Delta I'' = -21.1$ and $\Delta I' = -20.8 \mu\text{Å}^2$, respectively. Clearly, there is little or no change in the twist of the pyrrolidine ring relative to the benzonitrile ring upon excitation to the $S_1(^1L_b)$ state in PYRBN, as this would significantly affect the magnitude of the measured inertial defect relative to S_0 . This is different from the

geometric changes observed in both PBN and DMABN upon excitation,²⁴ the reasons for which will be discussed later.

Stark effect measurements also were made on PYRBN. Independent simulations and linear least-squares fits of spectra taken in electric fields ranging from 85 to 423 V/cm yield the following measured EDMs; $\mu'' = 8.2$ and $\mu' = 10.5$ D, entirely along the a inertial axis of PYRBN.

DISCUSSION

Through the use of high-resolution microwave and electronic spectroscopy, the S_0 and S_1 geometries of PP,²³ PBN, ABN,²⁹ DMABN,²⁴ and PYRBN in the gas phase have all been determined. In addition, the lowest-lying excited electronic state of all five molecules is shown to be the 1L_b state. However, although electronic transitions to these excited states involve the same (by symmetry) molecular orbitals, the geometric consequences of such an excitation are quite different and depend on the nature of both the donor and acceptor.

In both PP and PBN, the pyrrole subunit may act as an electron donor if ICT occurs, while the phenyl subunit may act as the electron acceptor. Here, we find that both pyrrole derivatives exhibit a substantial twist between donor and acceptor subunits in S_0 , which is measured to be $\phi'' = 36^\circ$ for PP (see SI) and $\phi'' = 32^\circ$ for PBN. As evidenced by the abundance of low-frequency FC progressions in their vibrationally resolved FES, the minimum energy geometries in S_1 must be considerably different from those found in S_0 .^{19,20,23} We find here by measuring the S_0 and S_1 inertial parameters of PP and PBN that both molecules become more planar upon electronic excitation. In PP, $\phi' = 20^\circ$ when eight quanta of the torsional mode are excited. The twist angle at the zero-point vibrational level must therefore be less than 20° , as exciting higher quanta of the torsion in S_1 should lead to larger average twist angles. In PBN band 1, $\phi' = 14^\circ$ is found for the tentatively assigned electronic 1L_b origin. For both pyrrole derivatives, we have therefore measured remarkable changes in the ring twist angle upon excitation to the 1L_b states of $\Delta\phi = -16^\circ$ and $\Delta\phi = -18^\circ$, respectively. The energetic preference for a more planar structure must arise from improved conjugation between the ring π systems upon excitation, resulting also in an increase in the π bond order of the bond connecting the two conjugated rings.

These results are consistent with the earlier theoretical predictions of Haas and co-workers.^{3,5} These authors suggest that the excited state CT coordinate involves a distortion of the phenyl ring to a quinoidal (Q) or antiquinoidal (AQ) structure. Our results, which clearly pertain to eigenstates influenced by various minima on the excited state electronic surface, reveal that the CT coordinates of excited PP and PBN involve AQ phenyl ring distortion, which occurs as the structure becomes more planar. The “doorway” eigenstates observed here are influenced by a CT minimum on the excited state surface, providing a window into the intrinsic excited state properties of both PP and PBN.

Although the addition of a cyano group to the electron accepting benzene ring does not appear to significantly alter the preferred 1L_b geometry of the pyrrole derivatives, it does significantly lower the energy of the second excited state, 1L_a . This state makes its appearance at excitation energies only 400 cm^{-1} above the presumed 1L_b origin in PBN. Clearly, the energy gap $\Delta E(S_1, S_2)$ is smaller for PBN than for PP in the gas phase, as no large increase in fluorescence intensity at higher excitation frequencies was observed for PP.³⁰ The 1L_a state is more planar

Table 3. Experimentally Measured Permanent Electric Dipole Moments and Twist Angles of PP, PBN, ABN, DMABN, and PYRBN^a

molecule	excitation	μ'' (D)	μ' (D)	$\Delta\mu$ (D)	ϕ'' (deg)	ϕ' (deg)	$\Delta\phi$ (deg)
PP ^b	¹ B	−1.56(1)	0.94(1)	+2.50(1)	36	20	−16
PBN band 1 ^c	¹ B	3.43			32	14	−18
PBN band 2 ^c	² ¹ A	3.43	6.0(1)	+2.6(1)	32	13	−19
PBN band 3 ^c	² ¹ A	3.43	6.3(1)	+2.9(1)	32	9	−23
ABN ^d	¹ B	6.41(3)	7.30(3)	+0.79(4)	0	0	0
DMABN ^e	¹ B	7.9(1)	10.60(3)	+2.7(1)	0	25	+25
PYRBN	¹ B	8.23(3)	10.52(3)	+2.29(4)	6	6	0

^aMeasured in the gas phase. Standard deviations as determined from the fits are shown in parentheses. ^b μ data from ref 23. ^c μ'' calculated using MP2/aug-cc-pVTZ//M05-2X/6-31+G* theory, and μ' calculated from the appropriate experimentally derived dipole function (see SI). ^d μ data from ref 35. ^e ϕ data from ref 24.

than both the ground and first excited states of PBN, with a smaller twist angle of only $\phi' = 9^\circ$, yielding a decrease in twist angle upon excitation to S_2 of $\Delta\phi = -23^\circ$. The near planarity of this state measured in the gas phase corresponds well to the calculated structure of the quinoidal form of ¹L_a, designated ²¹A(Q).^{3,5} (The corresponding designation of the ¹L_b state is ¹¹B.) We hypothesize that the (nearly) planar ²¹A(Q) state identified here as the low-lying excited S_2 state of PBN is responsible for the red emission observed in Ar matrix experiments^{31–33} and acetonitrile clusters formed in a supersonic jet.³⁴

When local π system conjugation within the donor moiety is lost, the ground state twist between donor and acceptor is suppressed, as was found in the ground states of ABN, DMABN, and PYRBN. Instead, a large amount of electron density (i.e., a lone pair) is localized on the nitrogen atom of the amino group in ABN and DMABN, giving rise to nonzero inversion angles (analogous to the sp³ hybridization invoked to rationalize the pyramidal structure of ammonia). However, the optimized S_0 geometry of PYRBN (M05-2X/6-31+G*) has a locally planar NR₂ arrangement, with a small twist angle relative to the benzonitrile ring of $\phi' = 6^\circ$. No twist is observed in S_0 of ABN and DMABN; instead, they are pyramidalized at the amino nitrogen. The ground state inversion angles of these two molecules are reported as 34° ²⁹ and 14.6° ,²⁵ respectively.

The charge density localized on the donor amino nitrogen in the ground state is transferred, at least in part, to the entire benzonitrile acceptor in all three cases upon excitation to the S_1 state. (Assuming that the benzonitrile ring is the acceptor, rather than the cyano group itself, we estimate from the measured $\Delta\mu$ of DMABN that $\sim 0.2e$ is transferred from the amino N to the geometric center of the ring. Since $\Delta\mu$ of DMABN is the largest, this is the upper-bound for all three saturated donor species.) However, this results in a measurable change in the vibrationally averaged amino inversion angle upon excitation only in the case of DMABN, on the basis of differences in the measured inertial defects of the S_0 and S_1 states.²⁴ In ABN, the two inertial defects are nearly the same,²⁹ but this parameter is much less sensitive to the geometry of the amino group in this case, owing to the smaller mass of the two hydrogens compared with the two methyl groups. In addition, in DMABN, the dimethylamino group twists to an angle of $\phi' = 25^\circ$, placing one methyl group above and the other methyl group below the benzonitrile plane. By allowing this twist, the dimethylamino group is able to stabilize a larger charge separation than in the case of ABN, which weakens the N–CH₃ bonds in S_1 relative to S_0 and decreases the barriers to internal rotation of the individual methyl groups.²⁴ A clear low-

frequency FC progression is observed in the vibrationally resolved FES of DMABN that is explained by the existence of unique geometries in S_0 and S_1 . In PYRBN, no change in twist angle is observed in S_1 , as indicated by the nearly identical inertial defects measured for each electronic state. The absence of low frequency activity in the vibrationally resolved FES of PYRBN is additional proof of little change in geometry upon excitation to the S_1 state.²⁶

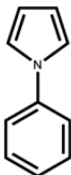
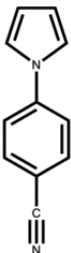
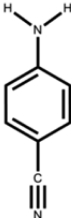
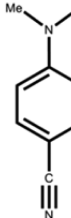
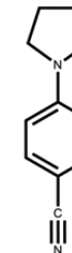
The consequences of increased or decreased donor–acceptor conjugation have been further explored by measuring the permanent EDMs of each molecule (see Table 3). The center of negative charge in the ground state of PP lies within the pyrrole ring, as evidenced by the orientation and magnitude of its permanent dipole, $\mu'' = -1.56$ D.²³ [The direction of the dipole (its absolute sign) is obtained from theory; experiment provides the magnitudes of the dipoles, and their relative signs.] Replacing the benzene ring in PP with the benzonitrile ring in PBN results in a change in both the magnitude and direction of its permanent EDM, $\mu' = 3.34$ D [a consequence of the larger dipole of benzonitrile itself ($\mu'' = 4.48$ D)],³⁵ again demonstrating the gas phase electron-withdrawing capabilities of the pyrrole subunit. Upon excitation to the ¹L_b state, the dipole of PP decreases in magnitude to $\mu' = 0.94$ D but reverses its vector direction because the center of negative charge now lies on the benzene ring acceptor. In contrast, the dipole of PBN increases in magnitude to $\mu' = 6.0$ D with no change in direction. Taking the relative signs into account, we see that the differences in the EDMs of the two states of PP and PBN are about the same, 2.5 and 2.6 D. The largest measured value of the EDM of PBN is that for the ²¹A state, $\mu' = 6.3$ D ($\Delta\mu = 2.9$ D). Even with the increase in spatial overlap between the π systems of each ring in the pyrrole derivatives, charge still moves from the donor to acceptor, which results in an increase in negative charge on the entire benzene and benzonitrile moieties, respectively.

The largest effect of π system conjugation, the sharing of electrons over the entire molecule, is made clear upon inspection of the μ_a dipoles measured for ABN, DMABN, and PYRBN. The ground state EDMs of all three molecules with saturated donor groups are large; $\mu'' = 6.41$ D for ABN,³⁵ $\mu'' = 7.9$ D for DMABN, and $\mu'' = 8.2$ D for PYRBN, much larger than those for PP and PBN. Evidently, extended conjugation decreases their ground state dipoles relative to their saturated-donor counterparts. Within the saturated-donor family, PYRBN has the largest μ'' , consistent with the geometric finding that its inversion angle of 0° (and therefore the amount of electron density on the donor nitrogen) is less than in DMABN (14.6°) and ABN (34°). More electron density from

the donor nitrogen is already present in the benzonitrile ring of PYRBN than in ABN or DMABN, which also necessitates a small but nonzero twist angle in the ground state of PYRBN.

Upon excitation to S_1 , the excited state EDMs of these three molecules are quite different. In ABN, $\mu' = 7.20$ D, a small change upon excitation of $\Delta\mu = 0.79$ D.³⁵ While the ground state EDMs of ABN and DMABN are effectively equal, the excited state EDM of DMABN is $\mu' = 10.6$ D, significantly larger than that found in ABN. For DMABN, $\Delta\mu = 2.7$ D for excitation to the S_1 state. For PYRBN, another large excited state EDM is found, with a measured value of $\mu' = 10.5$ D. However, the change in dipole upon excitation is slightly smaller than that of DMABN, at $\Delta\mu = 2.3$ D. In the case of ABN, some projection of the total EDM remains on the c inertial axis, partially explaining the small $\Delta\mu$ observed relative to DMABN and PYRBN. However, the fact that the NH_2 donor does not reach planarity upon excitation shows that a smaller amount of charge is transferred to the benzonitrile group in ABN than in the other two cases. In both DMABN and PYRBN, a twist exists in S_1 . While more dramatic in DMABN, the change in dipole moment upon excitation is similar to that of PYRBN, suggesting that electronically, the S_1 states of these two molecules are similar. When little or no twist exists in the ground states of the saturated donor molecules, the twist angle either remains the same or increases in their excited states. Chart 2 summarizes the dipole moments (in Debye) and twist angles of the S_1 states of all five molecules discussed in this report.

Chart 2. Summary of Benchmark S_1 4-Aminobenzonitrile Data

				
PP	PBN	ABN	DMABN	PYRBN
$\mu' = 0.94$ $\phi' \leq 20^\circ$	$\mu' < 6.02$ $\phi' = 14^\circ$	$\mu' = 7.20$ $\phi' = 0^\circ$	$\mu' = 10.60$ $\phi' = 25^\circ$	$\mu' = 10.52$ $\phi' = 6^\circ$

The EDMs of both ABN and DMABN have been previously measured in solutions of cyclohexane, benzene, and 1,4-dioxane using time-resolved microwave conductivity (TRMC) and

fluorescence spectroscopy techniques.³⁶ There, the ground state dipole moment of 6.6 D determined for both ABN and DMABN is in moderate agreement with the gas phase data for ABN, but substantially different from that of isolated DMABN. In the S_1 state, the EDMs were measured to be 8.3 D for ABN, and 9.9 D for DMABN. The authors claim³⁶ that each S_1 dipole measured by TRMC is an upper limit to the EDM of the isolated molecule, particularly in the case of DMABN, for which the first excited state is hypothesized to be increasingly influenced by the onset of a higher excited state as solvent polarizability and polarity is increased. Using the same $\mu'' = 6.6$ D determined in ref 36, the S_1 EDM of DMABN was also determined by measuring the electric field-induced changes in absorption and emission spectra in a polymer film of PMMA.³⁷ There, the excited state EDM of DMABN was reported to have a value of 9.8–10 D.

The low-lying electronic surfaces of many of these donor–acceptor molecules have been well-studied by various theoretical methods. The highest-level ab initio work available in the literature for these compounds exists only for DMABN, for which the resolution-of-the-identity coupled-cluster singles-and-doubles method RI-CC2 was employed using a triple- ζ valence basis set TZVPP by Köhn and Hättig.³⁸ Here, the relaxed geometries of three states were optimized: the ground 1^1A state, the 1^1B state, and the 2^1A state. The ground state was predicted to have an amino inversion angle of 23° and a dipole moment of $\mu'' = 7.4$ D, both in excellent agreement with gas phase data of 14.6^{35} and $\mu'' = 7.9$ D. Predictions for the 1^1B state also are in excellent agreement with experiment: the inversion angle is now 0° and a slight twist of the dimethylamino group was calculated to be $\phi' = 19^\circ$. The predicted dipole moment of $\mu' = 10.1$ D is slightly smaller than the experimental value of $\mu' = 10.6$ D. It is possible that this difference reflects some substantial motion along the ICT coordinate, since the FES of DMABN exhibits a significant Lorentzian contribution to the line width,²⁴ but in general, the RI-CC2 calculations do an adequate job of reproducing the experimentally determined quantities of DMABN in both S_0 and S_1 . Their prediction of a twisted ($\phi' = 90^\circ$) 2^1A state therefore seems very plausible.

Several theoretical investigations using relaxed CASSCF excited state geometries and subsequent single-point CASPT2 calculations have been reported^{39,40} and recently have focused on the importance of quinoidalization to ICT phenomena (see Table 4).^{3,5} In DMABN, ICT is generally understood to arise from a twisted ICT state. However, in the pyrrole derivatives PP and PBN, two ICT states were predicted: one planar and one twisted. The authors conclude that both PICT and TICT may be possible in the pyrrole derivatives owing to the

Table 4. Theoretical Permanent Electric Dipole Moments and Twist Angles of PP, PBN, ABN, DMABN, and PYRBN^a

molecule	excitation	μ'' (D)	μ' (D)	$\Delta\mu$ (D)	ϕ'' (deg)	ϕ' (deg)	$\Delta\phi$ (deg)
PP	1^1B	−1.9	0.1	+2.0	36.8	19.4	−17.4
PBN	1^1B	3.5	2.8	−0.7	36.5	36.3	−0.3
PBN	$2^1A(Q)$	3.5	10.6	+7.1	36.5	0	−36.5
ABN	1^1B	6.2	6.0	−0.2	0	0	0
DMABN	1^1B	6.5	7.0	+0.5	0	0	0
DMABN	$1^1B(AQ)$	6.5	14.8	+8.3	0	90	+90
PYRBN ^b	1^1B	7.4	10.4	+3.0	0	0	0

^aAvailable CASSCF theoretical data for each electronic transition observed experimentally (refs 3 and 5). ^bData not available in the literature. Calculated here for both electronic states at the M05-2X/6-31+G*/CASSCF(12,10)/D95 V level for comparison (see SI).

existence of an additional donor orbital within the π system of pyrrole. In the case of PBN, experiment clearly shows that a planar minimum exists on the S_2 surface, corresponding to the $2^1A(Q)$ structure predicted in the above-mentioned work. However, we find no experimental evidence for a second minimum of the $2^1A(AQ)$ variety, predicted to possess a larger dipole moment that would be further stabilized as an ICT state in solution. A comparison between CASSCF theory and experiment is made in Table 3.

Although DFT methods offer a significant reduction in computational cost relative to ab initio theories, improving their predictive success for relaxed geometries in excited electronic states is still an active area of research.⁴¹ Recently, the inability of standard DFT methods to accurately calculate the potential energy surfaces of excited states due to variations in the overlap of occupied and virtual orbitals as a function of geometry has been addressed by Wiggins et al.⁴² using a Coulomb-attenuated functional approximation (CAM-B3LYP). This promising technique, performed only on DMABN up to this point, should also be tested on the potential energy surfaces of other charge transfer systems with experimental and theoretical data readily available in the literature, such as those reported here.

SUMMARY

The transformation of reactant into product during an intramolecular charge transfer (ICT) process can involve several different potential energy surfaces (LE, ICT, etc.). Additionally, the connections between them can involve conical intersections along different vibrational coordinates. But all of these surfaces support molecular eigenstates to which contributions are made from the different canonical structures. Thus, studies of the electronic spectra of doorway states to ICT at high resolution could provide information about these dynamics despite the fact that such spectra are “vertical” and obey the Franck–Condon principle, since rotational motion may be slow compared to the time scales of interconversion.

The present study reveals new information about such processes in a family of 4-aminobenzonitriles, absent the perturbations produced by neighboring solvent molecules. We have measured the rotationally resolved electronic spectra of PBN, DMABN, and PYRBN in the presence of an electric field. These measurements, along with several supporting microwave spectroscopy experiments, provide the moments of inertia of each molecule in their ground and excited states as well as their gas phase permanent electric dipole moments in both electronic states. Thereby probed are the differences in the equilibrium geometries of the two states and the changes in charge distribution that are responsible for them.

We find that excitation of PP and PBN by light changes their structures from twisted ones to more planar ones, whereas excitation of ABN and PYRBN by light has little effect on their structures. In contrast, DMABN twists upon excitation by light and becomes more planar along the amino inversion coordinate. Despite these differences, the changes in electron distribution in all five molecules are about the same: $\Delta\mu = 2.0 - 2.7$ D in PP, PBN, DMABN, and PYRBN. Only in ABN is $\Delta\mu$ smaller; $\Delta\mu$ appears to be larger in the 1L_a state of PBN. The excited state permanent electric dipole moments of molecules containing para cyano groups are substantially larger than those without them; these change by more than an order of magnitude on going from PP to PYRBN. Thus, whether the PICT or TICT model applies to charge transfer processes in these systems seems to depend on the extent to which the

donating nitrogen atom (or group containing it) has a localized lone pair and whether the ground state molecule is twisted. Further high resolution experiments should address the extent to which these findings are modified by the attachment of weakly bound solvent molecules, thereby making a still stronger connection to the extensive condensed phase ICT literature.

ASSOCIATED CONTENT

Supporting Information

Theoretical details, microwave spectra and assignments, twist angle analysis, dipole correlation analysis, and the complete ref 17 are included. This material is available free of charge via the Internet at <http://pubs.acs.org>.

AUTHOR INFORMATION

Corresponding Author

*E-mail: pratt@pitt.edu.

Present Addresses

[‡]JILA, National Institute of Standards and Technology and University of Colorado, Boulder, Colorado 80309.

[†]Department of Chemistry, University of Vermont, Burlington, VT 05405.

Notes

The authors declare no competing financial interest.

ACKNOWLEDGMENTS

A. Held, S. Humphrey, J. McCombie, J. Ribblett, W. Sinclair, and M. J. Walker assisted with early zero-field experiments on PYRBN; L. Alvarez-Valtierra, J. W. Young, and C. L. Clements assisted with later electric field experiments on various molecules. We thank them for their help, and also thank J. P. Simons and J. A. Thomas for insightful discussions about this work. This research was supported by the Andrew Mellon Predoctoral Fellowship Program at the University of Pittsburgh (A.J.F.) and by grants from the National Science Foundation (CHE-0960074, B.H.P.; CHE-0911117, D.W.P.). It is dedicated to the memory of Paul Barbara, a leading contributor to the field of charge transfer, and a good friend.

REFERENCES

- (1) Grabowski, Z. R.; Rotkiewicz, K.; Rettig, W. *Chem. Rev.* **2003**, *103*, 3899–4031.
- (2) Lakowicz, J. R. *Principles of Fluorescence Spectroscopy* (3e); Springer: New York, 2006.
- (3) Zilberg, S.; Haas, Y. *J. Phys. Chem. A* **2002**, *106*, 1–11.
- (4) Gomez, I.; Reguero, M.; Boggio-Pasqua, M.; Robb, M. A. *J. Am. Chem. Soc.* **2005**, *127*, 7119–7129.
- (5) Cogan, S.; Zilberg, S.; Haas, Y. *J. Am. Chem. Soc.* **2006**, *128*, 3335–3345.
- (6) Majewski, W. A.; Pfanstiel, J. F.; Plusquellic, D. F.; Pratt, D. W. In *Laser Techniques in Chemistry*; Myers, A. B., Rizzo, T., Eds.; Wiley: New York, 1995, p 101.
- (7) Korter, T. M.; Borst, D. R.; Butler, C. J.; Pratt, D. W. *J. Am. Chem. Soc.* **2001**, *123*, 96–99.
- (8) Mitchell, D. M.; Morgan, P. J.; Pratt, D. W. *J. Phys. Chem. A* **2008**, *112*, 12597–12601.
- (9) Miller, D. M. Ph.D. Thesis, University of Pittsburgh, 2010.
- (10) Plusquellic, D. F. Ph.D. Thesis, University of Pittsburgh, 1992.
- (11) Plusquellic, D. F.; Suenram, R. D.; Mate, B.; Jensen, J. O.; Samuels, A. C. *J. Chem. Phys.* **2001**, *115*, 3057–3067.
- (12) Bird, R. G.; Pratt, D. W. *J. Mol. Spectrosc.* **2011**, *266*, 81–85.
- (13) Alvarez-Valtierra, L.; Shipman, S. T.; Neill, J. L.; Pate, B. H.; Lessari, A. In *The Ohio State University International Symposium on*

Molecular Spectroscopy; The Ohio State University: Columbus, OH, 2008, WF12.

(14) Emilsson, T.; Gutowsky, H. S.; de Oliveira, G.; Dykstra, C. E. *J. Chem. Phys.* **2000**, *112*, 1287–1294.

(15) Kisiel, Z.; Kosarzewski, J.; Pietrewicz, B. A.; Pszczolkowski, L. *Chem. Phys. Lett.* **2000**, *325*, 523–530.

(16) Kisiel, Z.; Bialkowska-Jaworska, E.; Desyatnyk, O.; Pietrewicz, B. A.; Pszczolkowski, L. *J. Mol. Spectrosc.* **2001**, *208*, 113–120.

(17) Frisch, M. J. et al. *Gaussian 03*; Gaussian, Inc.: Wallingford, CT, 2004.

(18) Dunning, T. H., Jr.; Hay, P. J. In *Modern Theoretical Chemistry*; Schaefer, H. F., III, Ed.; Plenum: New York, 1977; Vol. 3, pp 1–27.

(19) Belau, L.; Haas, Y.; Rettig, W. *Chem. Phys. Lett.* **2002**, *364*, 157–163.

(20) Okuyama, K.; Numata, Y.; Odawara, S.; Suzuka, I. *J. Chem. Phys.* **1998**, *109*, 7185–7196.

(21) Watson, J. K. G. In *Vibrational Spectra and Structure*; Durig, J. R., Ed.; Elsevier Scientific Publishing Company: New York, 1977; Vol. 6, pp 1–89.

(22) Platt, J. R. *J. Chem. Phys.* **1949**, *17*, 484–495.

(23) Thomas, J. A.; Young, J. W.; Fleisher, A. J.; Alvarez-Valtierra, L.; Pratt, D. W. *J. Phys. Chem. Lett.* **2010**, *1*, 2017–2019.

(24) Nikolaev, A. E.; Myszkiewicz, G.; Berden, G.; Meerts, W. L.; Pfanstiel, J. F.; Pratt, D. W. *J. Chem. Phys.* **2005**, *122*, 084309(1–10).

(25) Bird, R. G.; Neill, J. L.; Alstadt, V. J.; Young, J. W.; Pate, B. H.; Pratt, D. W. *J. Phys. Chem. A* **2011**, *115*, 9392–9398.

(26) Howells, B. D.; Martinez, M. T.; Palmer, T. F.; Simons, J. P.; Walters, A. J. *Chem. Soc., Faraday Trans.* **1990**, *86*, 1949–1956.

(27) Walker, M. J. Ph.D. Thesis, University of Nottingham, 1993.

(28) Caminati, W.; Dell'Erba, A.; Maccaferri, G.; Favero, P. G. *J. Mol. Spectrosc.* **1998**, *191*, 45–48.

(29) Berden, G.; van Rooy, J.; Meerts, W. L.; Zachariasse, K. A. *Chem. Phys. Lett.* **1997**, *278*, 373–379.

(30) Kobayashi, T.; Futakami, M.; Kajimoto, O. *Chem. Phys. Lett.* **1986**, *130*, 63–66.

(31) Schweke, D.; Haas, Y. *J. Phys. Chem. A* **2003**, *107*, 9554–9560.

(32) Schweke, D.; Baumgarten, H.; Haas, Y.; Rettig, W.; Dick, B. J. *Phys. Chem. A* **2005**, *109*, 576–585.

(33) Schweke, D.; Haas, Y.; Dick, B. J. *Phys. Chem. A* **2005**, *109*, 3830–3842.

(34) Belau, L.; Haas, Y.; Rettig, W. *J. Phys. Chem. A* **2004**, *108*, 3916–3925.

(35) Borst, D. R.; Korter, T. M.; Pratt, D. W. *Chem. Phys. Lett.* **2001**, *350*, 485–490.

(36) Schuddeboom, W.; Jonker, S. A.; Warman, J. M.; Leinhos, U.; Kuehnle, W.; Zachariasse, K. A. *J. Phys. Chem.* **1992**, *96*, 10809–10819.

(37) Yoshizawa, T.; Iwaki, Y.; Osaka, N.; Nakabayashi, T.; Zachariasse, K. A.; Ohta, N. *J. Phys. Chem. B* **2004**, *108*, 19132–19139.

(38) Köhn, A.; Hättig, C. *J. Am. Chem. Soc.* **2004**, *126*, 7399–7410.

(39) Serrano-Andres, L.; Merchán, M.; Roos, B. O.; Lindh, R. *J. Am. Chem. Soc.* **1995**, *117*, 3189–3204.

(40) Proppe, B.; Merchán, M.; Serrano-Andres, L. *J. Phys. Chem. A* **2000**, *104*, 1608–1616.

(41) Li, R.; Zheng, J.; Truhlar, D. G. *Phys. Chem. Chem. Phys.* **2010**, *12*, 12697–12701.

(42) Wiggins, P.; Williams, J. A. G.; Tozer, D. J. *J. Chem. Phys.* **2009**, *131*, 091101(1–4).